42p.

MTP-AERO-63-47
June 19, 1963

GEORGE C. MARSHALL SPACE FLIGHT CENTER

HUNTSVILLE, ALABAMA

STUDIES ON ABLATION OF OBJECTS TRAVERSING AN ATMOSPHERE

By

Ernst W. Adams, John D. Warmbrod, and Benton K. Berry

NATIONAL AERONAUTICS AND SPACE ADMINISTRATION

GEORGE C. MARSHALL SPACE FLIGHT CENTER

MTP-AERO-63-47

STUDIES ON ABLATION OF OBJECTS TRAVERSING AN ATMOSPHERE

By

Ernst W. Adams, John D. Warmbrod, and Benton K. Berry

ABSTRACT

This report reviews theoretical studies performed by the Aeroballistics Division with regard to the ablation-type heat protection of vehicles traversing an atmosphere. These studies rest on numerical solution methods of the pertinent partial differential equations representing balances of mass, momentum, and heat. Provided sufficiently small steps are used, the numerical calculation methods yield exact solutions for homogeneous and noncharring materials. This report presents major conclusions from these ablation studies; the details appear in twenty-three papers published by Aeroballistics Division between 1959 and 1963.

AUTHOR

GEORGE C. MARSHALL SPACE FLIGHT CENTER

MTP-AERO-63-47

June 19, 1963

STUDIES ON ABLATION OF OBJECTS TRAVERSING AN ATMOSPHERE

by

Ernst W. Adams, John D. Warmbrod, and Benton K. Berry

AERODYNAMICS ANALYSIS BRANCH
AEROBALLISTICS DIVISION

TABLE OF CONTENTS

DEFINITION OF SYMBOLS

SYMBOL	DEFINITION
A	Arbitrary level factor that the vapor pressure is multiplied with
a mm	Distance from surface to station where temperature is 1000°F
$b = c(t_e)$ mm	Distance from surface to station where any prescribed temperature is reached at time t_e(sec)
c(t) mm	Time-dependent distance from surface to station where any prescribed temperature is reached.
c_p kcal/kg°K	Specific heat
H km	Flight altitude
h_v kcal/kg	Heat of vaporization
k kcal/m°K sec	Thermal conductivity
$p_v(T)$	Vapor pressure function
$p_{v1}(T)$	Vapor pressure function assumed for tektite material
$p_{v2}(T)$	Vapor pressure function of fused silica
q_{bl} kcal/m^{2}sec	Heat blocked by evaporation and vapor diffusion
q_{aero} kcal/m^{2}sec	Aerodynamic heat transfer to evaporating surface
$\tilde{q}_{aero}$ kcal/m^{2}sec	Aerodynamic heat transfer to non-evaporating surface
R(t) mm	Time-dependent radius of ablating front face of tektite model
s mm	Time-integrated ablation rate
T °K	Absolute temperature
t sec	Time, t = 0 at entry point into atmosphere
V km/sec	Flight speed
v_∞ mm/sec	Ablation rate

DEFINITION OF SYMBOLS (Cont'd)

v_s mm/sec	Ablation rate due to evaporation of surface
W(t) gm	Time-dependent weight of tektite model
x mm or m	Coordinate measuring parallel to interface between shield and air
y mm	Coordinate measuring normal to interface
y^* mm	Coordinate y with origin fixed at surface before ablation begins
α 1/m	Absorption coefficient of glass
γ kg/m^3	Specific weight
ϵ	Emissivity constant for thermal radiation
Θ_i	Entry angle of flight trajectory into atmosphere, relative to earth's horizon
$\mu(T)$kg sec/m^2	Viscosity
μ^*	Arbitrary level factor that the viscosity is multiplied by

SUBSCRIPTS

e or f	Final flight time at impact on earth
i	Interface between shield and air

LIST OF TABLES

LIST OF ILLUSTRATIONS

GEORGE C. MARSHALL SPACE FLIGHT CENTER

MTP-AERO-63-47

STUDIES ON ABLATION OF OBJECTS TRAVERSING AN ATMOSPHERE

By Ernst W. Adams, John D. Warmbrod, and Benton K. Berry

SUMMARY

This report reviews theoretical studies performed by the Aeroballistics Division with regard to the ablation-type heat protection of vehicles traversing an atmosphere. These studies rest on numerical solution methods of the pertinent partial differential equations representing balances of mass, momentum, and heat. Provided sufficiently small steps are used, the numerical calculation methods yield exact solutions for homogeneous and noncharring materials. This report presents major conclusions from these ablation studies; the details appear in twenty-three papers published by Aeroballistics Division be tween 1959 and 1963.

SECTION I: INTRODUCTION

In support of the Army Ballistic Missile Agency's development work on the Jupiter missile and on satellites, the Fluid Dynamics Section of the Aeroballistics Laboratory was assigned in January 1958 to study the aerothermodynamics of ablation-type heat protection devices. With the exception of Reference 27, only experimental results and empirical relations for the effective heat of ablation were known at that time. For this reason, the purpose of the work to be done by the Fluid Dynamics Section was defined early in 1958 as follows: (1) to gain a better understanding of the heat rejection mechanism in ablation-type shields, (2) to study the transient characteristics of this mechanism along flight trajectories, and (3) to determine the merits, disadvantages, and limitations of different types of ablative heat protection devices. Since initially only two and later four men were assigned to work on this problem, the ablation studies were restricted to the analysis of the transient heat and mass flows in homogeneous and noncharring materials which are mathematically tractable. Relations for heat and mass transfer at the ablating surface were supposed to be known from pertinent boundary layer solutions. The first step, therefore, consisted of the derivation of rigorous numerical calculation methods which necessarily involve the solution of partial differential equations and thus demand computer evaluations. These calculation methods were employed in 1959 and 1960 to study the performance of various glass and Teflon heat shields attached to several reentry bodies of revolution flying at zero angle of attack. The change of mission that

accompanied the transfer of this organization from ABMA to NASA on July 1, 1960, brought about a change of emphasis and left part of the initial program uncompleted. The continuation of the theoretical ablation studies by the Fluid Dynamics Section after July 1, 1960, was governed by the following purposes: (1) to augment and finish work on some particularly important phases of the initially outlined program of ablation studies, (2) to fill a request from the Jet Propulsion Laboratory for supporting work on the preliminary design of a Mars entry vehicle, (3) to fill a request from the Ames Research Center for rigorous numerical solutions pertaining to ablating glassy bodies, and (4) to fill a request from the Goddard Space Flight Center for supporting work on the aerothermodynamics of tektite flight in order to contribute new aspects to this problem in space physics.

SECTION II. CALCULATION METHODS

A. Methods Derived and Employed

The flows of heat and mass in objects ablating under conditions of hypersonic flight are governed by partial differential equations of the boundary layer type which represent the balances of mass, momentum, and heat. These equations are strongly nonlinear because of the temperature dependency of the material properties. Table 1 lists the numerical solution methods which have been derived and applied for the case of homogeneous and noncharring materials. The numerical methods (1) - (3) in the following are exact insofar as the numerical errors can be shown to tend to zero uniformly together with step sizes:

(1) A transient difference method with two independent variables has been derived for the stagnation point of a melting and evaporating shield. This method is applicable at any cross section downstream of the stagnation point if flows of heat and mass parallel to the surface are negligible.

(2) A transient difference method with three independent variables has been derived for any cross section of a melting and evaporating shield of a body of revolution flying at zero angle of attack.

These difference methods employ specially adapted procedures in the vicinity of the shield-air interface, where temperature gradients of the order of 1000°K/mm are encountered during ablation of glass shields under conditions of hypersonic entry. The calculation of melt flow in method (2) is sensitive to discontinuities of the mathematical expressions for the gradients $p'(x)$ or $\tau_i'(x)$ of pressure and interface shear stress, respectively, at the transition station x_o of body segments possessing different geometric configurations, e.g., spherical nose and conical frustum. The following calculation method, with time as the only independent variable, is rigorously valid if the surface does not ablate and if heat conduction is restricted to the surface normal.

(3) The surface temperature is obtained from solving an integro-differential equation, whose solutions are good approximations to results of methods (1) and (2) in case of nonmelting but evaporating surfaces.

Ablation type materials respond to high heating rates with high rates of surface radiation and/or mass transfer both in the molten and the gaseous states. For this reason, the net heat transfer rate across the surface is very much smaller than the gross amount of heat incident at the surface, provided this gross rate is sufficiently high. If this is true, the surface temperature may be approximated with a high degree of accuracy by ignoring both the preceding heating and ablation history and the net heat transfer rate as compared to the individual fluxes contributing to this net rate. Therefore, the following approximate calculation method has been derived and applied:

(4) The surface temperature is obtained from solving a time-independent ordinary equation which represents "radiation and mass transfer equilibrium."

The initial program on ablation studies included the derivation of a Karman-Pohlhausen integral solution to serve as an engineering calculation method for surfaces which melt and evaporate under transient conditions. This plan has not been carried out because of the transfer from ABMA to NASA on July 1, 1960.

B. Comparison of Transient and Quasi-Steady Calculation Methods

Table 2 presents a list of typical objects whose descending flight across earth's atmosphere has been analyzed by use of the calculation methods of Section IIA. Data for the stagnation points of the IRBM and the satellite appearing in Table 2 have been calculated by use of the transient method (1) in Section IIA and by use of the quasi-steady method presented in Ref. 1. Figure 1a shows the flight speeds, V, of these vehicles as functions of both altitude and entry time. Fig. 1b presents the surface temperatures, T_i, Fig. 1c the ablation speed v_∞, and Fig. 1d the distance a between the surface and the station where the temperature is 1000°F at the end of the flight. Since the quasi-steady analysis rests on a radiation and ablation balance of the incident heat, this method must fail before ablation begins. This is confirmed by the three performance graphs, Figures 1b, 1c, and 1d. As a check on the accuracy of the calculation methods involved, one notices their close agreement during the ablation period.

SECTION III. GENERAL CONCLUSIONS OF ABLATION STUDIES

A. Review of the Problem

The derived calculation methods have been employed to study the performance of shields made of glasses or of Teflon in case of selected

entry flights which cover the total range of missile, satellite, and space vehicle trajectories in the earth's atmosphere. In addition, the ablation process of stony meteorites has been studied numerically to supplement the field of small and moderate ablative mass losses of entry vehicles; this extension more clearly establishes trends in the variation of vehicle and trajectory parameters.

The governing criterion for the heat protection of any vehicle traversing an atmosphere at hypersonic speed is the ratio of heat shield weight to the total weight of the vehicle. At minimum weight, a heat protection device should keep both the temperature and the heat transfer at its inner surface below specified bounds. Therefore, as much of the incident aerodynamic and radiative heat transfer as possible should be returned into the air flow adjacent to the shield with the smallest possible ablative mass loss.

If any object traverses an atmosphere in hypersonic, descending flight, the rates of both the aerodynamic and radiative heat fluxes incident at the surface are significant only when the flight speed is sufficiently high. Table 2 presents the altitude ranges in which aerodynamic heat transfer and ablation are encountered by typical objects traversing the earth's atmosphere. Because of the relatively small flight speed reached at the end of the heating period, heating and ablation occur only during a small fraction of the total flight time in the atmosphere. With the exception of cases like short-range missiles, however, the magnitude of the peak heat transfer rate does not permit the utilization of heat shields only as heat sinks.

Table 3 presents a list of available heat protection materials. The calculation methods listed in Section II have been applied to glasses as typical high-temperature ablators and to Teflon, a typical low-temperature ablator. In the following three sections, several particularly important aspects of ablation type heat protection shields are discussed. In section IIIB, the merits and disadvantages of high- and low-temperature ablators are treated. Ablation by mass transfer and ablation by melt flow are compared in section IIIC. Section IIIB deals with transparent and nontransparent materials.

B. High Versus Low Ablation Temperatures

While available ablation type materials do not possess well defined temperatures at which the pertinent changes of state occur, temperature ranges always exist in which the ablation phenomena take place. If melt flow and evaporation of the heat shield's constituents occur only at high temperatures, the ablative mass loss is relatively small. For these so-called high-temperature ablators, radiation from the shield into the air may provide a significant decrease of the shield's heat absorption. This type of heat transfer back into the air is desirable, since it does

not involve any loss of shield material. High surface temperatures evidently require sufficiently small values of the thermal diffusivity and relatively short flight durations in order to avoid thick, and thus heavy, shields. If thermal stresses are disregarded, glass shields may survive heat pulses of extremely high magnitude and sufficiently brief duration. Glass-protected surfaces, therefore, can cope efficiently with the intense and short-lasting heat pulses characteristic of steep high-speed entry flights. Since, in general, the terminal flight period after the end of the ablation pulse is short on these trajectories, the conduction of previously absorbed heat across the shield remains within tolerable bounds during this period.

The performance of a low-temperature ablator is characterized by approximately equal progress rates of the ablating surface and the thermal penetration of the shield. While the heated layer thus is thin, the ablative mass losses are relatively large and radiation emitted from the shield is insignificant in general. Since radiative heating incident at the surface in general is not absorbed by the gas released from an evaporating or sublimating surface, a low-temperature ablator is likely to fail entirely if exposed to radiative heating; i.e., catastrophic ablation rates may be expected then. (A high-temperature ablator, though, can cope efficiently with both aerodynamic and radiative heating modes provided the material is opaque to radiation.) These disadvantages are compensated for by the fact that some low-temperature ablators are considerably better thermal insulators than available high-temperature ablators; e.g., Teflon, possesses a thermal diffusivity which is about one order of magnitude smaller than the one of glasses. Teflon shields, therefore, can cope with long-lasting aerodynamic heat pulses of low magnitude which, however, exceed the limit tolerable for nonablating radiation-cooled shields. This type of heating is experienced on nearly horizontal entry trajectories with small deceleration rates.

C. Ablation by Mass Transfer Versus Ablation by Melt Flow

The heat of evaporation or sublimation absorbed at the surface of a shield under conditions of aerodynamic, i.e., convective and/or radiative heating, constitutes a continuously distributed heat sink at the shield-air interface. In addition, mass transfer reduces the convective heat transfer in case of a laminar air boundary layer flow by influencing the velocity and temperature profiles. This beneficial effect is considerably smaller in case of turbulent boundary layer flow. Also, vapor emitted by an ablating surface in general is very nearly transparent to the radiation of the gas cap behind the shock wave.

The flow of melt in a layer adjacent to the surface of an ablating shield transports heat absorbed by the shield. The melt flow in general proceeds in the direction of the air flow adjacent to the shield and solidifies in regions with small heat transfer downstream

of the stagnation point. Instabilities of the melt flow, particularly where the deceleration of the entry vehicle causes a local reversal of the melt flow's direction, may cause a spraying of melt. While mass transfer decreases the aerodynamic heat transfer across the laminar boundary layer, melt flow in general removes hot melt from the vicinities of maximum heat input, and thus causes a more uniform distribution of the heat penetrating the shield.

Some detrimental effects of mass transfer on calculated heat shield performance have been shown in References 12 and 13 for a quartz shield mounted on a space vehicle traversing the earth's atmosphere under the conditions listed in Table 2. If it were possible to suppress evaporation at the stagnation point, the necessary shield thickness could be decreased from 76 to 64 mm at that point. This is explained by the calculated result that the nonevaporating opaque shield reaches a maximum surface temperature of 4623°K and removes 95 percent of the incident convective heat at the stagnation point by surface radiation, whereas the evaporating shield reaches a maximum temperature of 3101°K and radiates only 28 percent back into the air.

The evaporation of the quartz shield for this space vehicle reentry is very sensitive to increases in the aerodynamic heat transfer. When the heat transfer coefficient at the stagnation point of the evaporating shield is increased by a constant factor 2 during the entire flight, the total ablated thickness rises by a factor of 2.4, while the necessary thickness of the shield increases by a factor 1.65. When the heat transfer coefficient is increased by the same factor 2 at a distance of 4 meters downstream from the stagnation point, where ablation is negligible, the necessary thickness of the shield rises by only 5 percent. If the heat transfer coefficient is increased by the factor 2 at the stagnation point of the nonevaporating quartz shield, the necessary thickness increases only by 8 percent.

It may be concluded that the large mass transfer on the nose of this reentry vehicle keeps the surface temperature at such a comparatively low level that radiative cooling cannot govern the cooling balance. Decidedly contrary to mass transfer cooling, this radiative cooling possesses the desirable insensitivity to increases in the heat transfer incident at the surface.

D. Transparent Versus Nontransparent Materials

The effects of radiative heat exchange, in addition to the transportation of heat by convection and conduction in the shield, have been studied at the shield's stagnation point axis of symmetry by (1) considering convective heating only, (2) ignoring reflection and scattering of radiation, and (3) neglecting any net radiative flux across a cylinder surrounding the stagnation point axis. Because of the last assumption,

calculation method 1 in Section II is applicable after adding pertinent terms to the energy balance, so that this differential equation then becomes an integro-differential equation. The modified calculation method 1 has been employed to study the influence of internal radiation in case of a space ship, whose flight data are listed in Table 2, and in case of cylindrical glass rods under axial heating and ablation conditions. The results of this study are presented in Table 4 and Figure 2. The experimental data for the Pyrex rod in Figure 2 have been obtained by courtesy of Dr. Dean R. Chapman of the Ames Research Center, NASA. Unfortunately, the absorption coefficient α of the test specimen is not known. Calculations were therefore carried out for the absorption coefficient of clear window glass, $\alpha = 100$, and the one of opaque material, $\alpha = \infty$. The comparison of experimental and calculated ablation data reveals satisfactory agreement, as is seen in Figure 2.

The analysis of the calculated cases yields the following conclusions pertaining to changes of α, the only material parameter affecting radiant heat exchange:

(1) In general, both the surface temperature and the surface temperature gradient decrease together with α, causing lower temperatures in a layer adjacent to the surface and higher temperatures elsewhere.

(2) Correspondingly, when α is changed, the rate of melt flow may increase or decrease, whereas the evaporation rate changes together with α.

(3) The time-dependent length $c(t)$ is defined as the distance between the surface and that station in a semi-infinite shield where any prescribed temperature is reached. This parameter $c(t)$ can be used to determine the necessary thickness of the shield. Item (1) of this list shows that $c(t)$ may increase or decrease upon any change of α. If the heating pulse stops a sufficient time before the end of the flight ($t = t_e$), the parameter $b = c(t_e)$ increases as α is reduced.

This list is confirmed by the results presented in Table 4. It is seen that both the residual thickness b of the shield and its total necessary thickness $(s + b)$ at the stagnation point of the space ship increase as α decreases. However, $(s + b)$ decreases together with α in case of the rods made of Pyrex glass and quartz, where b and s pertain to the time instant the heating pulse terminates.

The so-called effective, apparent, or fictitious thermal conductivity has been employed frequently in the past to calculate superimposed radiative and conductive heat fluxes by use of a substituting heat conduction mechanism. Mathematical solutions and experiments express the effective thermal conductivity under stationary conditions as dependent on the geometry of the problem and as proportional to the third power of the

absolute temperature. Because of the high temperatures encountered and the transient character of heat shield performance under entry conditions, use of the effective thermal conductivity gives grossly deviating results as compared to studies properly accounting for conductive and radiative transport of heat.

E. The Influence of Individual Glass Properties on Shield Weight

The necessary thickness of the glass needed on the shield to protect the vehicle is the sum of the total ablation s and the residual thickness b needed as a heat sink between the final surface and the supposedly thermally insulated inner edge. This thickness b is determined by the restriction that the thermally insulated inner edge never reaches a temperature larger than 460°K at any time during the reentry. The necessary weight $\gamma(s + b)$ is the weight per unit area of the required glass shield, where γ is the specific weight of the glass.

The effect of the material properties of glass on the necessary weight was studied for many glass shields, each with a different set of assumed properties, in case of the IRBM, ICBM, and the satellite listed in Table 2. Figures 3 and 4 present some results of this study.

The thermal properties of the glass shields were varied as follows:

(1) thermal conductivity k, $0.61 \times 10^{-4} \leq k \leq 9.713 \times 10^{-4}$ (kcal/m°K sec),

(2) specific heat c_p, $0.10 \leq c_p \leq 0.58$ (kcal/kg°K),

(3) emissivity constant ϵ, $0.10 \leq \epsilon \leq 0.8$ (-),

(4) viscosity level of Pyrex glass μ^*, $0.10 \leq \mu^* \leq 100$ (-), and

(5) vapor pressure level of Pyrex glass A, $0 < A \leq 1000$ (-).

A and μ^* are constants that the vapor pressure and viscosity functions $p_v(T)$ and $\mu(T)$, respectively, of Pyrex glass were multiplied by in order to study the effect of these material parameters.

Experimental results for opaque Pyrex glass show that $k/\gamma c_p$ the relevant combination of k, γ, and c_p, slightly decreases with increasing temperatures; e.g., T = 473°K yields $k/\gamma c_p = 7.9 \times 10^{-7} m^2/sec$ and T = 1073°K yields $k/\gamma c_p = 7.3 \times 10^{-7}$ m^2/sec. The results presented in Figures 3 and 4 were calcuated by assuming k, γ, and c_p as constants. In order to check the effect of this assumption on k, γ, and c_p, the necessary weight of a quartz shield for the space ship reentry listed in Table 2 was also calculated by using curve fits for the material properties k = k(T) and $c_p = c_p(T)$.

The results have been compared with a case where mean constant values for the two properties k and c_p were employed. Both cases yielded approximately the same value of the necessary weight.

Figure 3 shows the total ablation s, the heat sink thickness b, and the necessary thickness (s + b) for the IRBM reentry as functions of k, c_p, and the viscosity level factor μ^* for Pyrex glass. It is evident from this graph that small values of k, large values of c_p, and large values of μ^* are desirable properties of glass shields in order to minimize the necessary weight. Similar graphs for the ICBM and the satellite show the same trend.

Figure 4 shows the effect of the material properties on the necessary weight at the stagnation point of the glass shields for three reentries listed in Table 2 as a function of the thermal diffusivity $k/\gamma c_p$. The shaded areas show for each reentry the range of necessary weights that result from varying the thermal properties between the previously mentioned limits. It is evident from this graph that $k/\gamma c_p$ is the most influential material parameter on the necessary weight for all of the investigated reentries if $k/\gamma c_p$ has the desirable small values and/or ablation is insignificant. This is verified by the calculated results which show for given material properties that the IRBM experiences the smallest and the ICBM the largest ablative mass loss. As $k/\gamma c_p$ increases, the temperature profile normal to the surface spreads, and thus the molten layer becomes thicker. Correspondingly, the influence of each individual material property k, c_p, ϵ, μ, and p_v on $\gamma(s + b)$ increases together with $k/\gamma c_p$.

Numerical solutions for heat shield performance on ballistic entry trajectories show that large percentages of both the time-integrated surface radiation and the time-integrated mass transfer rates are concentrated in the short-lasting, high-temperature ranges. According to these calculations, changes of all the relevant material properties have only very little effect on the surface temperature in this range because of the strongly nonlinear temperature dependencies of the material properties and of the Stefan-Boltzmann radiation law. For a given thermal diffusivity, then, the temperature profile normal to the surface of an opaque shield depends only weakly on changes in ϵ, p_v, and μ.

The numerical solutions also indicate that any increase of ablative mass losses by melt flow or evaporation due to property changes are compensated for to a large extent by a smaller heat absorption in heat sink fashion and thus also a smaller thermal penetration of the shield. This explains, e.g., why changes of the vapor pressure level A in the bounds $0 < A \leq 10^3$ influence the necessary shield thickness (s + b) only within the limits ± 7 percent, as solutions for the four reentry vehicles listed in Table 2 show.

SECTION IV. CALCULATED RESULTS FOR INDIVIDUAL RE-ENTRY FLIGHTS

A. Space Ship Traversing the Atmosphere of the Earth

The performance of quartz and Teflon shields was studied for a space ship traversing the atmosphere of the earth (see Ref. 12). The

capsule is presented in Figure 5a, the entry parameters appear in Table 2. The capsule possesses a spherical nose of one meter diameter followed by a conical frustum of 3.69 meters in length with a largest diameter of 3.77 meters. This capsule has a volume of 18 m^3 and weighs 8640 kg. The ballistic factor is 500 lb/ft^2 under the assumption of a mean drag coefficient c_D of 0.32. The reentry point was placed at the altitude of 120 km above sea level where both aerodynamic and radiative heating are still negligible.

Calculations have been made at the stagnation point for both a compact quartz shield and one with 50 percent porosity, hereafter called foamed quartz shield. While the specific weights differ by a factor 2, the thermal diffusivities $k/\gamma c_p$ were assumed equal. Also, transportation of heat by radiation across the inner cavities was excluded. The results show that both shields experience approximately the same weight loss per unit area at the stagnation point. In order not to exceed the prescribed temperature of 460°K at the shield's insulated inner edge, the compact shield needs to have a thickness of 44 mm while the foamed shield needs only 39 mm because the surface temperature distributions are approximately equal, and the smaller thermal conductivity of the foamed material causes larger surface temperature gradients. The necessary weight per unit area of the compact shield at the stagnation point therefore exceeds the one of the foamed shield by a factor 1.66. In order to minimize the change in the vehicle's shape, the ablating outer layer of the quartz shield should be compact, while the inner layer must be porous for small shield weight.

The performance of a foamed quartz shield and a Teflon shield have been analyzed on the spherical and the conical parts of the capsule surface. The calculations indicate that 99 percent of the quartz's ablative mass loss is due to evaporation so that the calculation method No. 1 in Section IIA is applicable for the entire body. Figures 5b and 5c present for the quartz shield the surface temperature and the vapor flow, respectively, as functions of time and distance x from the stagnation point. The subsidiary graph in Figure 5b shows the time when the assumed transition Reynolds number of 10^6 is reached at station x_{tr}. The second peak of heat transfer and surface temperature occurs immediately after transition, and results in negligible ablative mass of the quartz shield. On the conical frustum of the Teflon shield, however, 40 percent of the total mass loss takes place after transition has been reached.

Figures 6a and 6b present the surface temperatures at the stagnation point of the foamed quartz shield and the Teflon shield, respectively, as functions of time t and distance y^* normal to the surface. It is seen that Teflon ablates considerably faster than quartz at the stagnation point. Because of both a smaller thermal diffusivity and a more rapid rate of surface recession, the temperature profile in the Teflon shield is considerably steeper than the one in the quartz shield. Accordingly, the Teflon shield absorbs significantly less heat than the quartz shield.

Figure 7 shows the necessary weight of the quartz shield and the Teflon shield as functions of x. Since the heat shield performance on the nose is governed by the ablative mass loss, the quartz shield weighs less than the Teflon shield on the nose. Because the heat absorption and thermal penetration are dominant on the frustum, the Teflon shield is lighter than the quartz shield there.

The effects of the thermal radiation incident at the surface of the space ship's heat shield have been ignored up to this point. Available pertinent data indicate that the gas radiation incident at the stagnation point amounts to as much as 65 percent of the aerodynamic heat transfer to a cold wall for the reentry flight under discussion. If the quartz shield is nontransmittent to thermal radiation, its necessary thickness at the stagnation point increases by only 16 percent; this is explained by the fact that the maximum surface temperature at the stagnation point rises only from 3101°K to 3161°K when the gas radiation is added to the aerodynamic heat transfer at the stagnation point of the quartz shield.

B. Capsule Traversing the Atmosphere of Mars

The unmanned Mars probe consists of a spherical nose and a conical afterbody. The maximum diameter is 0.814 m and the overall length 1.28 m. The entry parameters at the altitude of 300 km above Mars' surface (entry time zero) are listed in Table 2. The flight velocity decreases from 6.5 to 1 km/sec in the period 40 to 80 sec, followed by a long period of low-speed flight to impact at 210 sec. This gives a short pulse of intense aerodynamic heating with a peak of 500 kcal/m^2 sec at the stagnation point during the period 30 to 80 sec, followed by a long period of negligible heating. Thus, a material for the heat shield has to be found which minimizes the sum of ablated thickness s and residual shield thickness b at impact time.

Four materials were considered for the ablation type heat shield: quartz, fiberglas, Teflon, and phenolic nylon. For quartz and fiberglas the calculation method no. 2 in section II A has been used, where fiberglas shield was approximated by a homogeneous model. Teflon and phenolic nylon decompose without forming a molten layer. A modification of calculation method no. 2 was needed to account in an approximate way for the formation of a char layer on an ablating shield made of phenolic nylon. Experimental results for the effective heat of ablation and the ablation temperature were used for the phenolic nylon calculations.

Even considering the most conservative of the available empirical expressions, phenolic nylon was found to make the lightest shield. The main advantages of phenolic nylon are its low thermal diffusivity, the high emissivity of the char formed by decomposition, and the fact that the decomposition forms gases of low molecular weight, which are more effective in heat blocking than gases of high molecular weight. Quartz

was the least effective shield material because it did not have enough vaporization for heat blocking at the temperatures reached, and its thermal diffusivity was so high it allowed a greater thermal penetration than the other materials.

The structure under the shield was supposed to act as a heat sink, thus helping the shield dissipate the absorbed heat. Two structure materials were considered, aluminum and fiberglas. When the shield is thick, the heat flux penetrating to the structure is small and distributed over a long time interval. This makes the structure's heat capacity more important than its thermal conductivity. On the conical section of the capsule, where only a thin shield is needed, the heat flux to the structure is in a short pulse. A high thermal conductivity of the structure is mandatory on the cone to dissipate the heat quickly. From these thermal considerations aluminum was found to make the lighter structure.

SECTION V. FLIGHT OF NATURAL QUARTZ OBJECTS IN THE EARTH'S ATMOSPHERE

A. Tektite Flight

Tektites are small glassy bodies which are found in Indochina, the Philippines, Indonesia, Australia, Texas, Georgia, Ghana, Bohemia, and Moravia. All tektites have a family-like chemical composition and are unrelated to the local geological formations; therefore, they must have been hurled up somewhere by violent natural events and carried in flight into the strewn fields. All the australites and some javaites belong to one of a few well-defined geometric shapes, which can be explained by ablation in hypersonic flight in the earth's atmosphere. It has not been possible yet to prove whether tektite flight started at the earth's surface or at some extraterrestrial point of departure. Chapman has presented conclusive experimental proof in Ref. 25 that glass spheres, when placed in an electric-arc jet tunnel and exposed to heating rates of the order of those experienced in hypersonic flight, become strikingly similar to the button-type australites (see Fig. 8). Chapman also has shown in Ref. 25 that an oscillation about any axis other than the flight axis is rapidly damped by the continuously increasing magnitude of the pressure distribution in descending flight, whereas this damping effect is absent in ascending flight.

Since the button-type australites then must have entered the earth's atmosphere as cold glassy spheres, ablation and trajectory analysis are applicable. Because the temperature level in tektites may take any values--whereas the temperature and the temperature gradient at the inner edge of the heat shield of a vehicle are subjected to upper bounds--the conclusions from the tektite study differ somewhat from the ones of vehicle studies. The results for the flight of the button-type australites to be presented in the following have been obtained under the assumption of a simplified geometrical model whose shape is determined by the stagnation point ablation

only. Experimental results show that radiative heating of objects as small as tektites is negligible in hypersonic flight. Fig. 9 presents, as functions of entry speed V_i and entry angle θ_i, curves of constant ratio of total heat blocked by mass transfer over total aerodynamic heat flux, both at the stagnation point. It is seen that more than 90 percent of the aerodynamic heating rate is blocked at high entry speeds. Calculations show that less than 20 percent of the total kinetic energy converted into heat enters the boundary layer surrounding the object. These considerations indicate why in Figure 10, which presents curves of constant relative mass loss as functions of entry speed and entry angle, spheres of only 11 grams initial weight may enter with as much as 26 km/sec in the vertical direction and still lose only 50 percent of their initial mass. (Both convective and radiative heating rates at entry speeds > 15 km/sec have been obtained by extrapolating correlation formulas valid for lower speeds.)

Table 5, which has been compiled by analyzing all the calculated results for tektite flight, explains the dependence of relevant parameters on entry speed V_i, entry angle θ_i, initial mass m(0), and the level of the vapor pressure of the material. This dependence is predominantly determined by the aerodynamic heating pulse and by the shield's mass transfer effect. A smaller percentage of the kinetic energy converted into heat reaches the surface as the heat pulse is shifted to lower altitudes, where a higher portion of the generated heat remains in the denser air. The case is clearest for the change of the entry angle θ_i, since this does not affect the total kinetic energy converted into heat. The following conclusions follow from Table 5:

(1) The relative mass loss increases as the initial mass m(0) decreases; i.e., the chance of survival drops together with the initial size of small objects.

(2) The relative mass loss increases only moderately together with the entry speed because the heat pulse is shifted to a higher altitude so that the mass transfer effect increases more rapidly than the surface temperature does. This explains why small objects can traverse the atmosphere at high entry speeds.

(3) As the trajectory becomes steeper (θ_i increases), the relative mass loss drops significantly since the time-integrated aerodynamic heating pulse, calculated as if the surface were cold, decreases strongly; from this it is seen that the chance of survival of small bodies is better on a steep than on a shallow--i.e., long-lasting--trajectory.

(4) As the level of the vapor pressure increases, a strong decrease of both the surface temperature and the relative mass loss takes place, while the mass transfer effect rises significantly. However, this decrease in relative mass loss is not true, in case of a reentering nose cone where the heated quartz layer is relatively small.

B. Meteor Flight

Since the thickness of the hot gas cap between the shock front and the surface of an object traversing the atmosphere in hypersonic flight increases together with the body's cross section, meteors are predominantly heated by equilibrium or nonequilibrium radiation from the hot gas cap, whereas bodies as small as tektites essentially experience convective heating only. Detailed calculations show that the extremely high radiation rates of as much as 10^4 - 10^6 kcal/m^2 sec, which are incident at the surface of a spherical meteor of 10^5 tons, cause the surface to boil. If the material is opaque to thermal radiation, the heated layer beneath the rapidly receding surface has a thickness of considerably less than 1 mm. The calculations show, however, that a layer of several centimeter thickness reaches temperatures of 3000 to 5000°K if the material is sufficiently transparent to thermal radiation. Vapor nuclei are then formed at nonhomogeneous spots in the glassy melt. Unless strong temperature gradients normal to the surface exist in the melt, there is no force present which drives the bubbles towards the surface. The outer portions of the radiatively heated layer therefore consist of a spongy glass melt, which offers little resistance to being removed from the meteor by the air forces acting in hypersonic flight. It may be concluded that the intensity of the gas radiation rates, which is comparable only to the ones liberated by nuclear explosions, causes any heavy object traversing the atmosphere in hypersonic flight to experience large mass loss rates regardless of the material's transparency to thermal radiation.

TABLE I

LIST OF CALCULATION METHODS

Number of Method	Number of Independent Variables	Number of Space Variables	Transient or Stationary	Method Furnishes Numerically Exact Solution Of	Characteristics of Numerical Solution	Solution Yields	General Remarks
1	2	1	Transient	3 Partial Differential Equations	Modified Difference Method	Temperature and Melt Flow Profiles, Surface Evaporation or Sublimation Rates	Applicable (a) in the vicinity of a stagnation point with or without radiant heat exchange (b) everywhere if the flows of heat and mass parallel to the surface are negligible and if radiant heating may be ignored.
2	3	2	Transient	3 Partial Differential Equations	Modified Difference Method	Temperature and Melt Flow Profiles, Surface Evaporation or Sublimation Rates	Applicable to any melting and evaporating shield of a body of revolution flying with zero angle of attack if the shield is non-transmittent to radiation.
3	1	0	Transient	Integro-Differential Equation for Surface Temperature	Step Method Proceeding in Time Direction	Surface Temperature and Evaporation or Sublimation Rates at Surface	(a) Method furnishes an exact solution for nonablating surfaces and one-dimensional heat conduction without radiant heat exchange in the shield. (b) Method yields good approximation up to the end of the ablation period if melt flow and radiant heat exchange in the shield are absent
4	0	0	Stationary	Ordinary Equation For Surface Temperature	Solution is Determined by Graphical or numerical methods	Surface Temperature and Evaporation or Sublimation Rates at Surface	Method is valid if the net heat flux across the surface is very much smaller than the individual contributions to the net heat flux and in the absence of melt flow and radiant heat exchange.

TABLE II

ALTITUDE RANGES OF AERODYNAMIC HEATING AND ABLATION PULSES

Entering Object as a Typical Representative of	Entry Angle Relative to Earth's (Mar's) Horizon	Entry Velocity (km/sec)	At the Stagnation Point					
			Aerodynamic Heating Values Pertain to Wall at 300°K				If Radiation of Shock Layer is Ignored	
			Aerodynamic Heating Begins to exceed 100 Kcal/m^2sec at Altitude (Km)	Aerodynamic Heating Reaches its Maximum at the Altitude (Km)	Aerodynamic Heating Becomes Smaller Than 100 Kcal/m^2sec at Altitude (Km)	Maximum Value of Aerodynamic Heating (Kcal/m^2sec)	Ablation of Quartz begins at Altitude (Km)	Ablation of Quartz Shield Ends at Altitude (Km)
IRBM	35°	4.5	67.5	25	12	840	36	10
ICBM	24°	7.226	86.5	20	5.9	6500	71	6
Satellite	2°	7.9	90	55	37	625	76	36
Space Ship	5°	11	96.6	47	23	2800	80	22
Tektite (Meteorite	6°	7	90.0	68	56	1000	75	51
Tektite (Meteorite	90°	30	106	61	37	248,895	92	37
Mars Vehicle	40	6.4	145	62	40	500	110	40

TABLE III

CLASSES OF ABLATORS

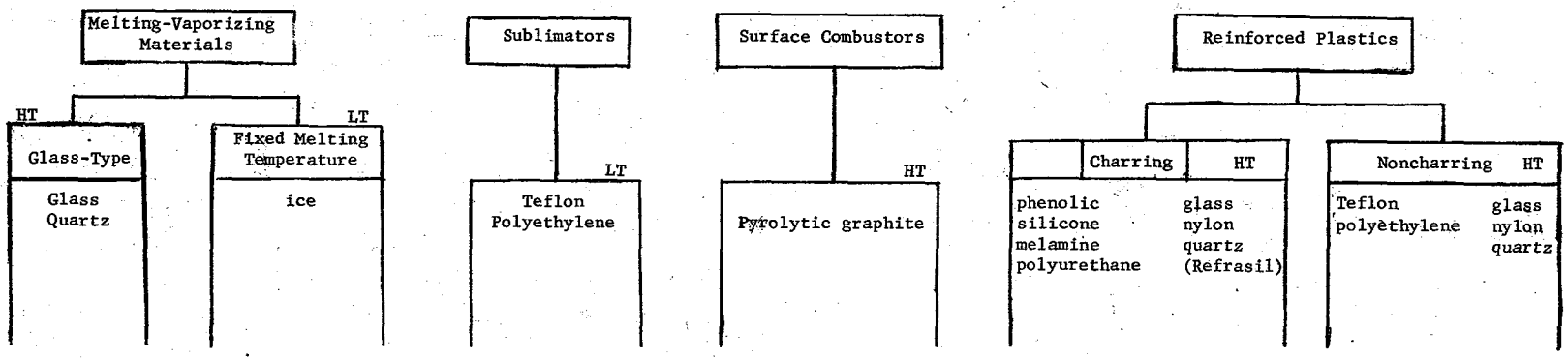

HT = High temperature ablator

LT = Low temperature ablator

TABLE IV

EFFECTS OF INTERNAL RADIATION AT STAGNATION POINT AXIS

Space Capsule with Quartz Shield Treated in Section IIIA				
Absorption Coefficient	1/m	100	200	∞
Maximum Surface Temperature at Stagnation Point	°K	2974.5	3023.0	3100.0
Evaporation Rate at Time of Maximum Surface Temperature	mm/sec	.0518	.0684	.1135
Distance c Between Surface and Station 460°K at Time of Maximum Surface Temperature	mm	39.85	45.0	2.013
Time-Integrated Ablation Rate	mm	5.46	9.48	19.117
Final Thickness b of shield	mm	81.01	63.0	43.86
Necessary Thickness (s + b) of Shield	mm	86.47	72.48	62.98

		Results for Axial Heating of Pyrex Cylinder		Results for Axial Heating of Quartz Cylinder	
Absorption Coefficient	1/m	100	∞	100	∞
Time Instant = Total Test Time	sec	10	10	10	10
Surface Temperature at t_e = 10 sec	°K	2068	2050	2589	2622
Distance b Between Surface and Station 460°K at t_e = 10 sec	mm	3.25	3.33	5.5	6.5
Time Integrated Calculated Ablation Rate s	mm	3.92	4.55	.48	.55
Time Integrated Experimental Ablation Rate s_1^*	mm	3.98		.39	
Distance (s + b) of Station 460°K from Original Surface	mm	7.17	7.88	5.98	7.05

TABLE V

GENERAL CONCLUSIONS DRAWN FROM THE ANALYSIS OF TEKTITE FLIGHT

The heat transfer parameter listed and the temperature pertain to the stagnation point.

Parameter	Change due to Increase of Entry Speed	Change due to Increase of Entry Angle	Change due to Increase of Mass at Entry Time	Change due to Increase of Vapor Pressure Level
Relative Mass Loss	moderate increase	strong decrease	moderate decrease	strong decrease
Aerodynamic Heat Transfer times Crossectional Area over kinetic energy converted into heat	small increase	small decrease		very small increase
Altitude where Maximum of Aero-dynamic Heat Pulse occurs	small increase	moderate decrease	small decrease	no change
Duration of Aero-dynamic heat pulse		strong decrease	moderate increase	no change
Maximum surface temperature	small increase	moderate increase	moderate increase	strong decrease
Maximum Aerodynamic heating rate	strong increase	strong increase	moderate increase	very small increase
Ratio of heat radia-ted from surface to Aerodynamic heating	moderate decrease	moderate decrease	nearly constant	strong decrease
Ratio of heat blocked by mass transfer to aerodynamic heating	moderate increase	small increase	very small increase	strong increase
Ratio of Evaporation to total ablation	moderate increase	small increase		strong increase

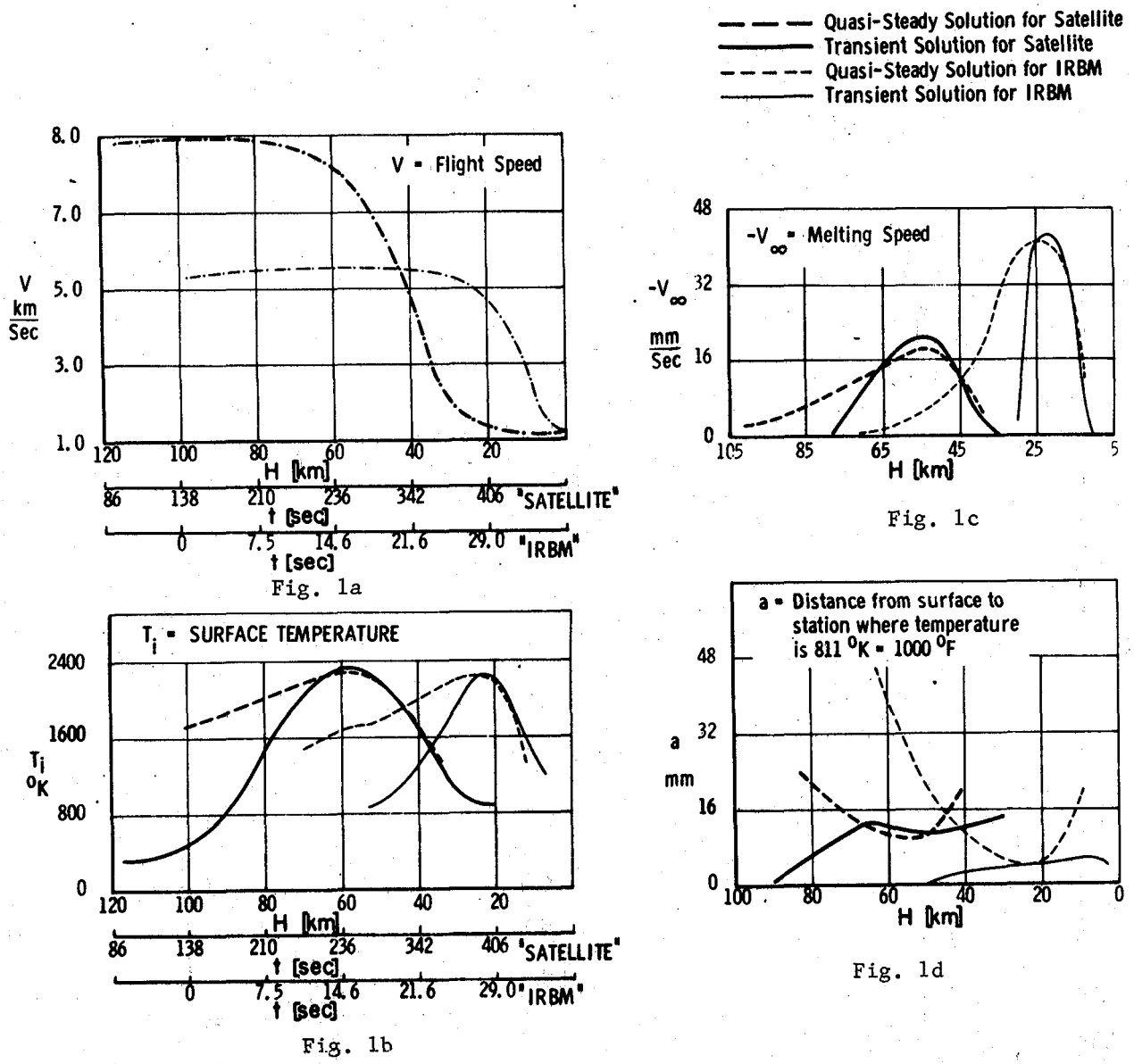

Fig. 1a

Fig. 1c

Fig. 1b

Fig. 1d

FIGURE 1: COMPARISON OF TRANSIENT AND QUASI-STEADY PERFORMANCE OF PYREX SHIELDS AT STAGNATION POINT OF IRBM AND SATELLITE

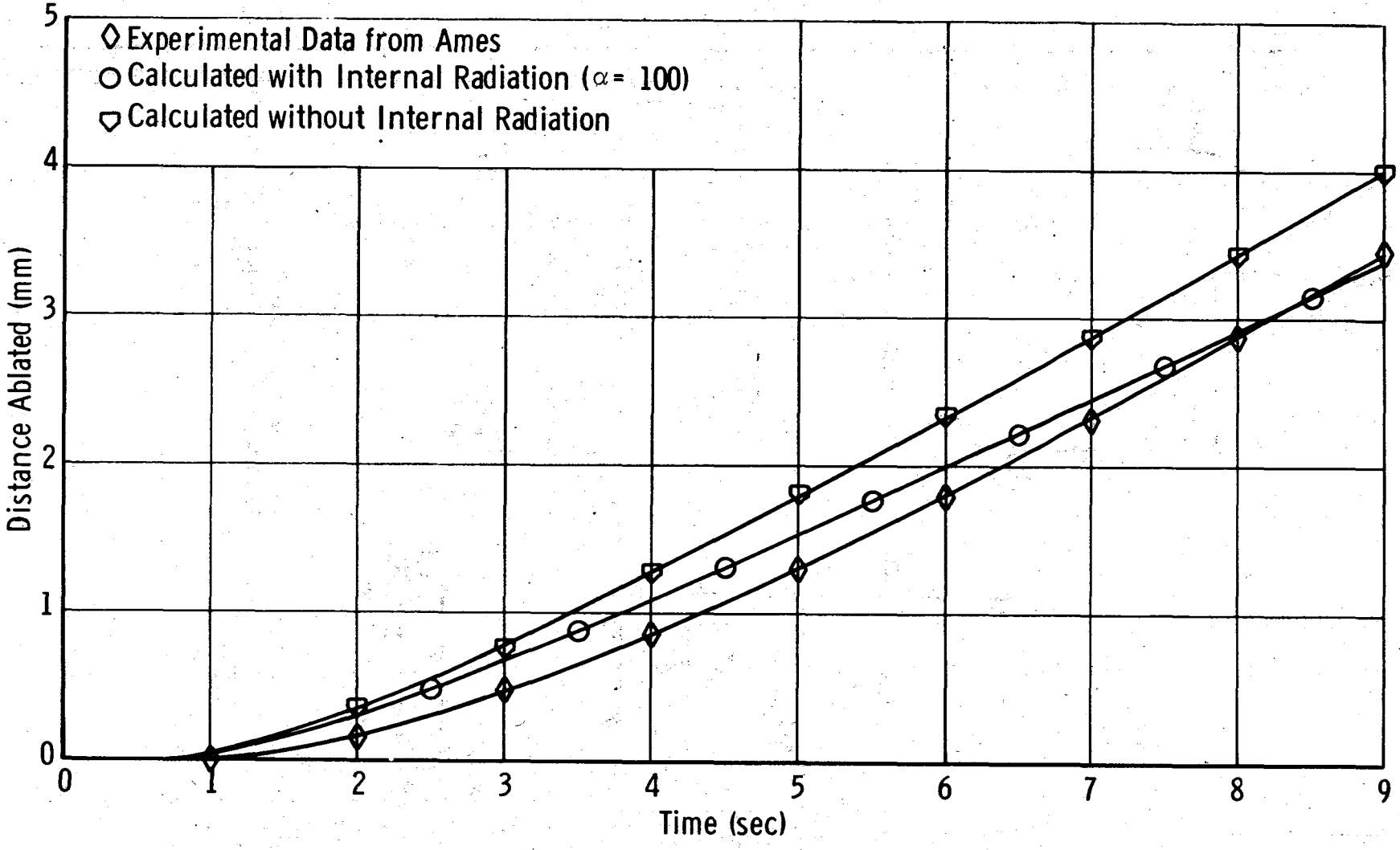

FIGURE 2: COMPARISON OF EXPERIMENTAL AND CALCULATED RECESSION OF SURFACE AT STAGNATION POINT OF PYREX CYLINDER

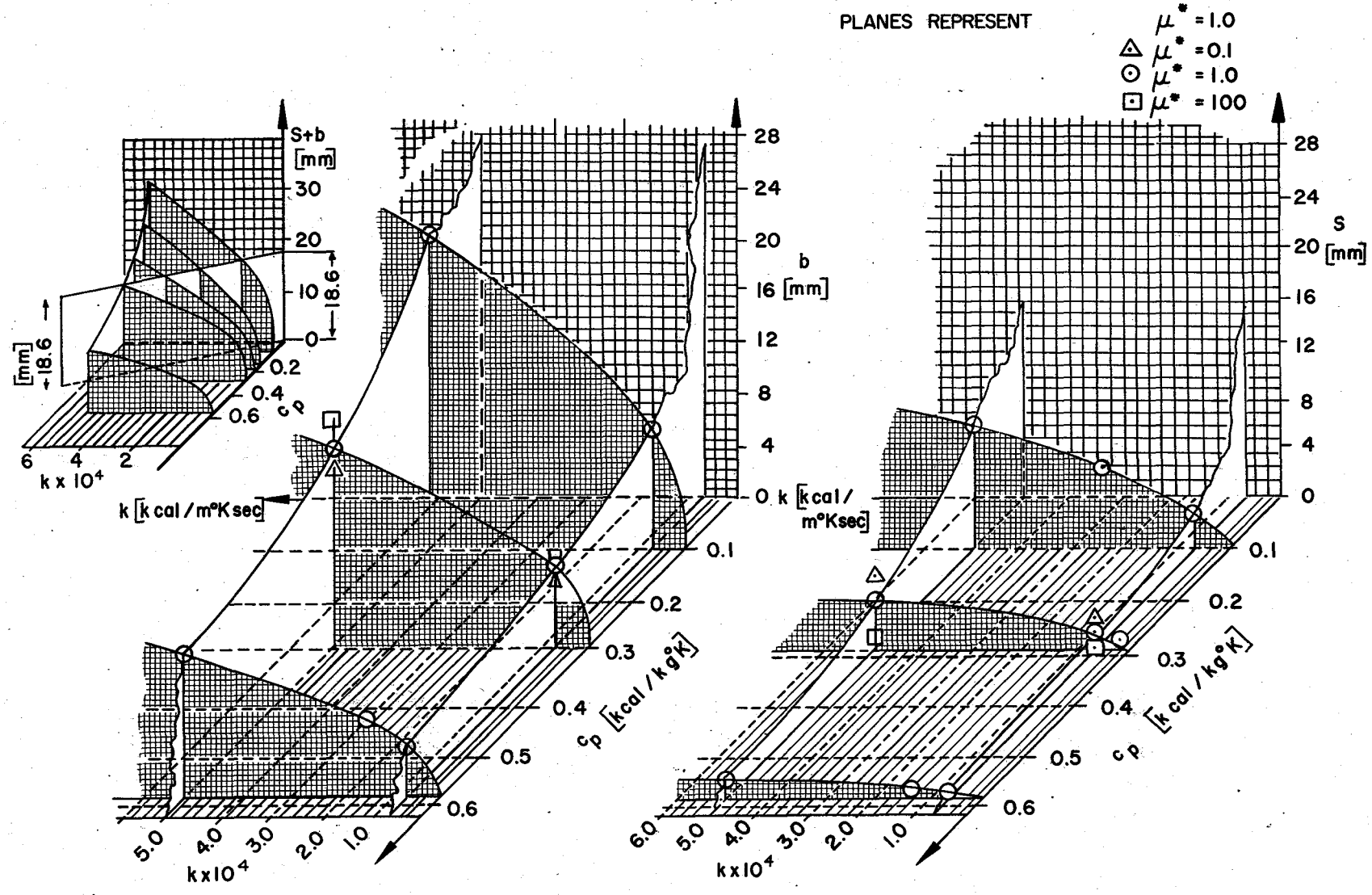

FIGURE 3 MAXIMUM THERMAL PENETRATION b AND TOTAL ABLATION s AT THE STAGNATION POINT OF AN IRBM

	IRBM	ICBM	SATELLITE
Entry Speed (m/sec)	4500	7226	7500
Entry Angle	35^0	24^0	2^0

Material Property Variations	
	$0.61 \times 10^{-4} \leq k \leq 9.713 \times 10^{-4}$ (kcal/m ^{0}K sec)
	$0.10 \leq c_p \leq 0.58$ (kcal/kg ^{0}K)
	$0.10 \leq \epsilon \leq 0.8$ (-)
	$0.10 \leq \mu^* \leq 100$ (-)
	$0 \leq A \leq 1000$ (-)

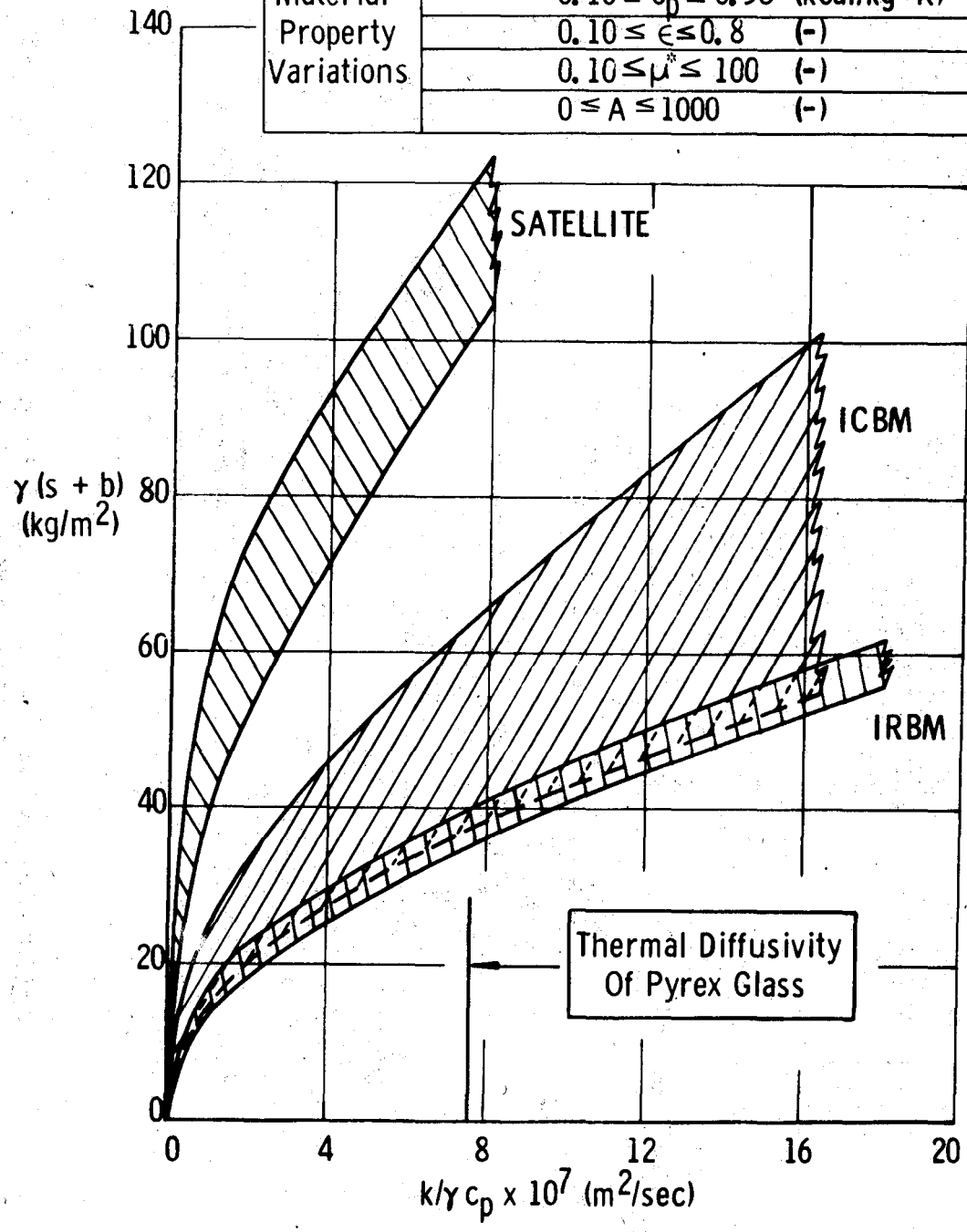

FIGURE 4: NECESSARY HEAT SHIELD WEIGHT AT STAGNATION POINTS OF THREE ENTRY VEHICLES

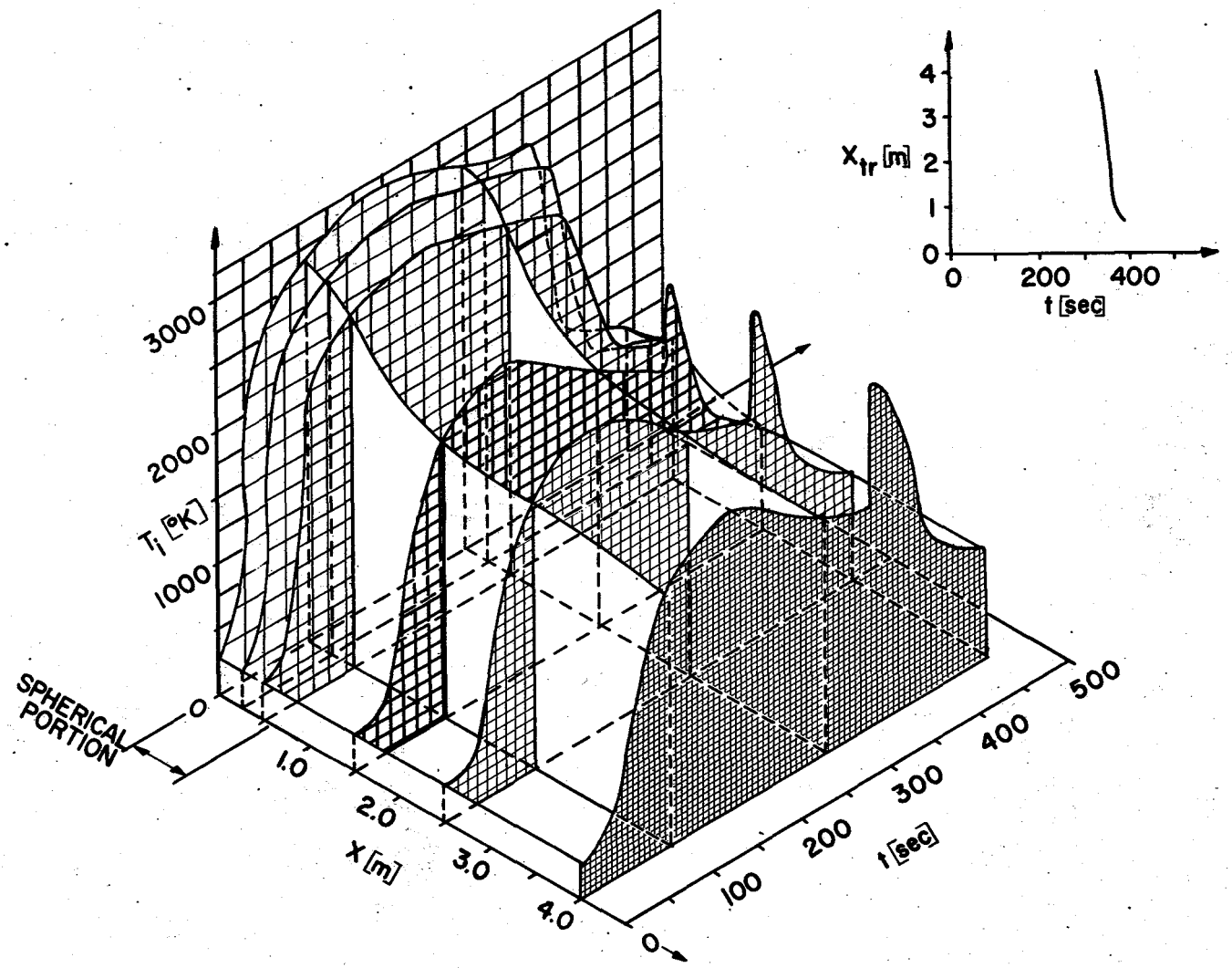

FIGURE 5A. SURFACE TEMPERATURE $T[x,o,t]$ FOR A QUARTZ SHIELD AND TRANSITION POINT $x_{tr}[t]$ OF THE AIR BOUNDARY LAYER (SPACE SHIP)

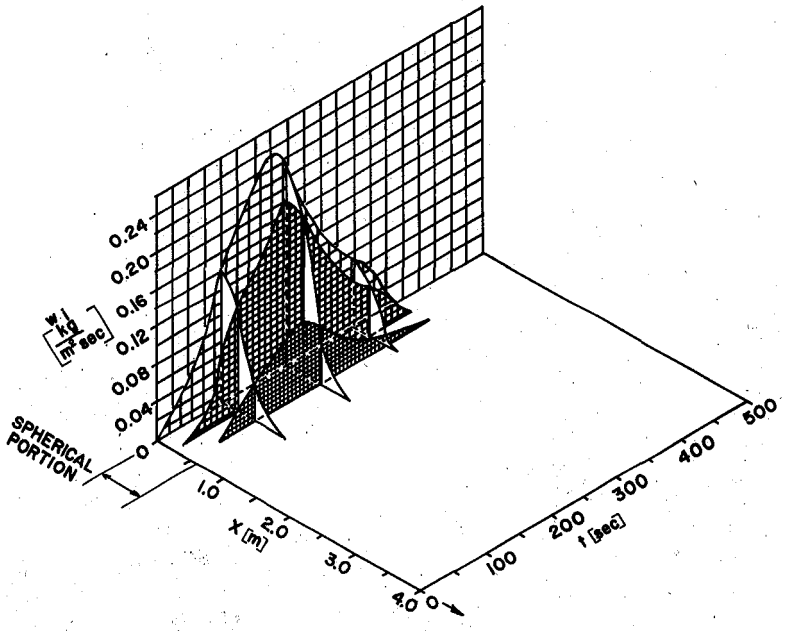

FIGURE 5 B. VAPOR FLOW $w_i(x,t)$ FOR A QUARTZ SHIELD (SPACE SHIP)

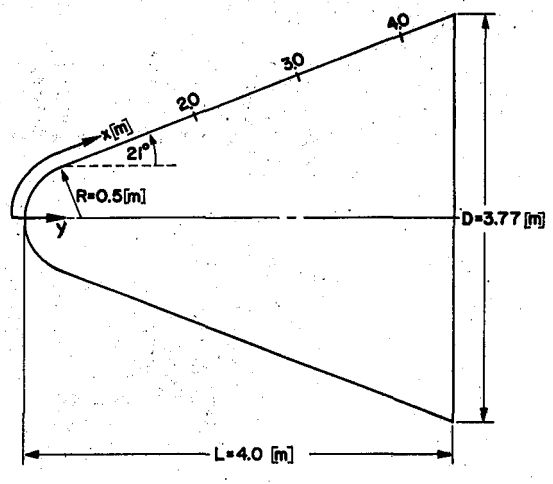

FIGURE 5C. CROSS SECTION OF SPACE SHIP

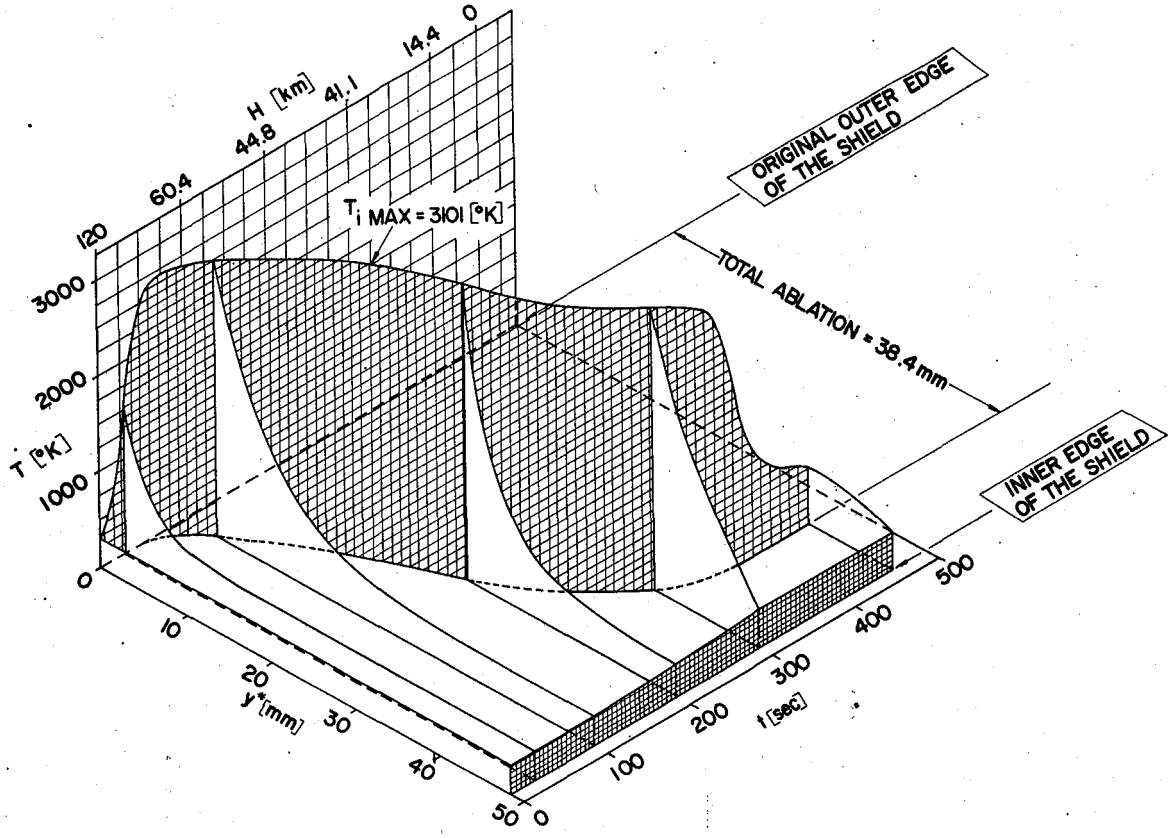

FIGURE 6a: TEMPERATURE DISTRIBUTION T[o,y*, t] FOR A QUARTZ SHIELD (SPACE SHIP)

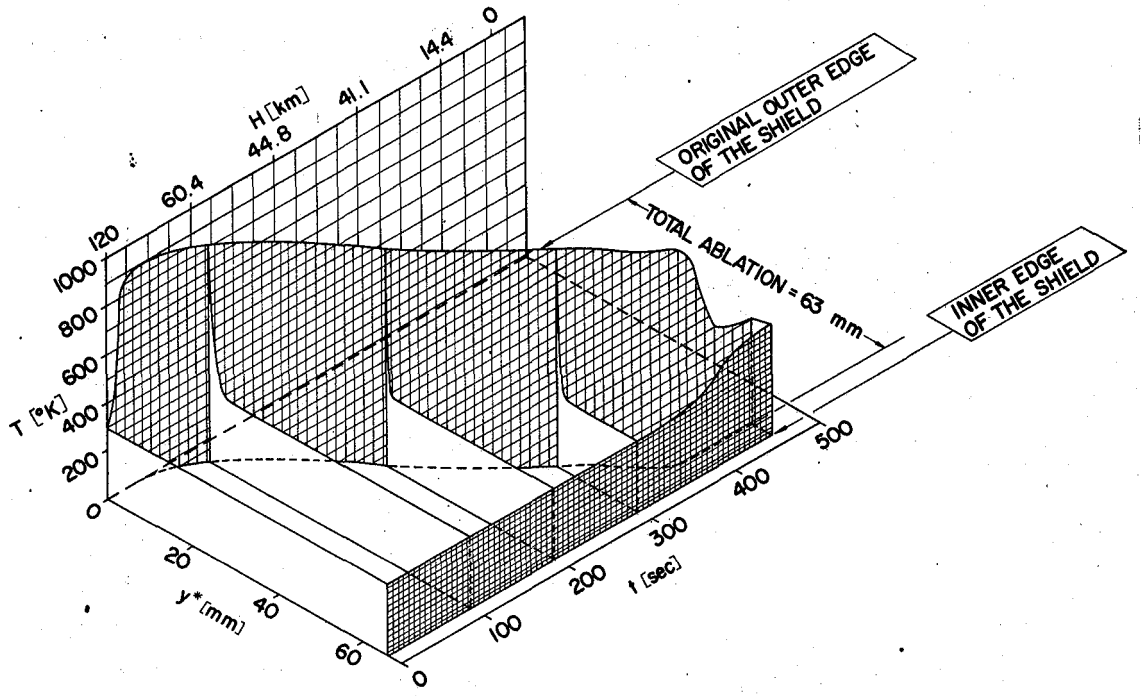

FIGURE 6b: TEMPERATURE DISTRIBUTION T[o,y*, t] FOR A TEFLON SHIELD (SPACE SHIP)

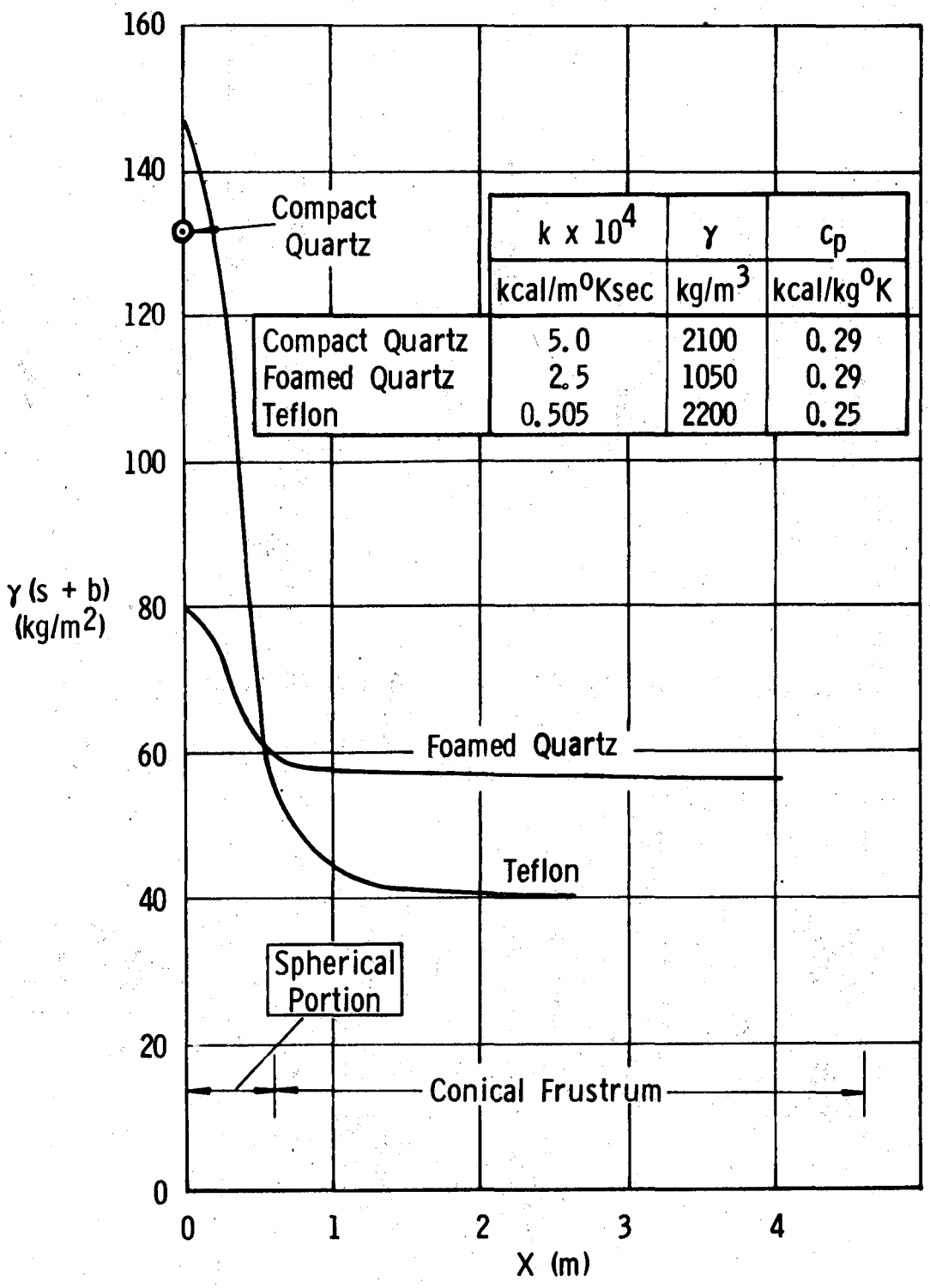

FIGURE 7: NECESSARY WEIGHT OF GLASS AND TEFLON SHIELDS AS FUNCTIONS OF DISTANCE X FROM STAGNATION POINT FOR RE-ENTERING SPACE VEHICLE

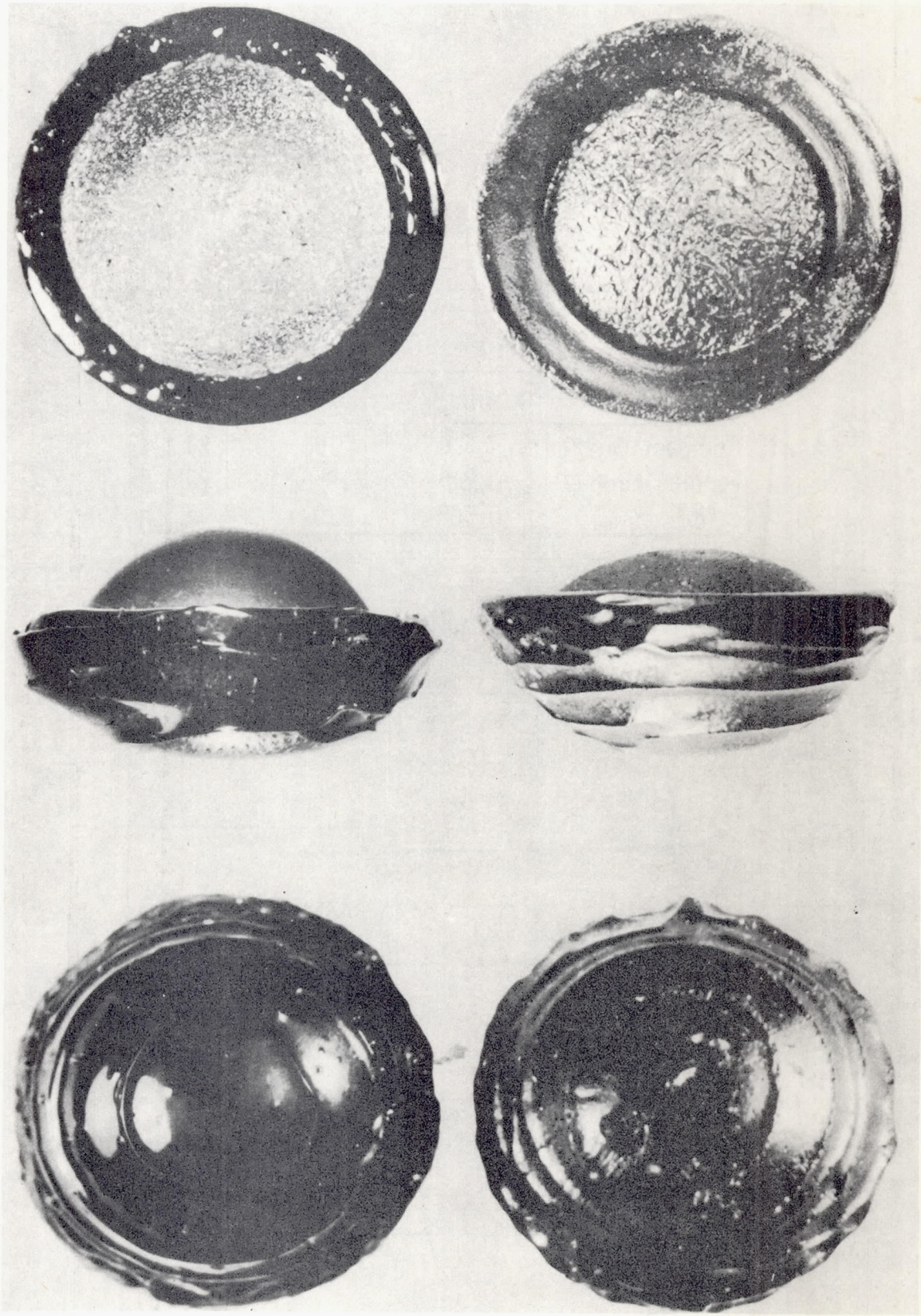

FIGURE 8: COMPARISON OF THREE AUSTRALIAN BUTTON TEKTITES (AT RIGHT, NOW IN BRITISH MUSEUM) WITH THREE TEKTITE GLASS MODELS (AT LEFT) ABLATED BY AERODYNAMIC HEATING

Data pertains to initially hemispheric model with:
Radius R(0) = 1.30 cm, i.e. W(0) = 11.04 grams, and vapor pressure $p_{v1}(T)$ (———)
Radius R(0) = 0.65 cm, i.e. W(0) = 1.38 grams, and vapor pressure $p_{v1}(T)$ (– – – –)
Radius R(0) = 1.30 cm, i.e. W(0) = 11.04 grams, and vapor pressure $p_{v2}(T)$ (—·—)
$q_{bl} = (\bar{q}_{aero} - q_{aero}) + \gamma h_v V_s$, where $\bar{q}_{aero} - q_{aero}$ is due to the diffusion of vapor across the boundary layer and $\gamma h_v V_s$ is the heat absorbed by the evaporation process.

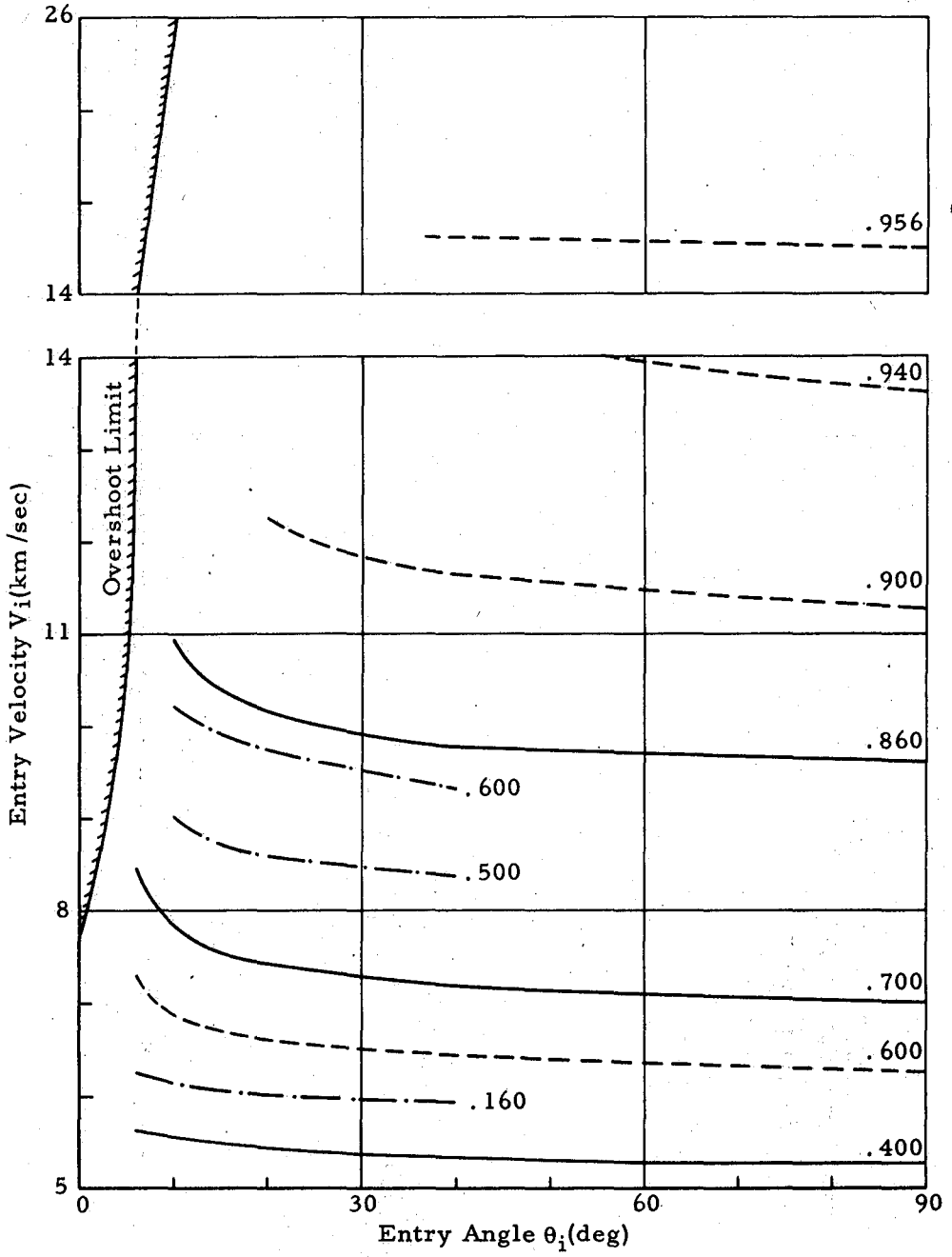

FIGURE 9: RATIO OF HEAT BLOCKED BY MASS TRANSFER EFFECT TO AERODYNAMIC HEATING, $\int_0^{t_f} q_{bl}\,dt \Big/ \int_0^{t_f} \bar{q}_{aero}\,dt$, AT THE STAGNATION POINT

(AUSTRALIAN BUTTON TEKTITE)

Data pertains to vapor pressure function $p_{v1}(T)$ and initially hemispheric model with mass m(0):
Radius R(0) = 1.30 cm, i.e. W(0) = 11.04 grams (———)
Radius R(0) = 0.65 cm, i.e. W(0) = 1.38 grams (– – – –)
$m(t_f)$ = final mass at impact time

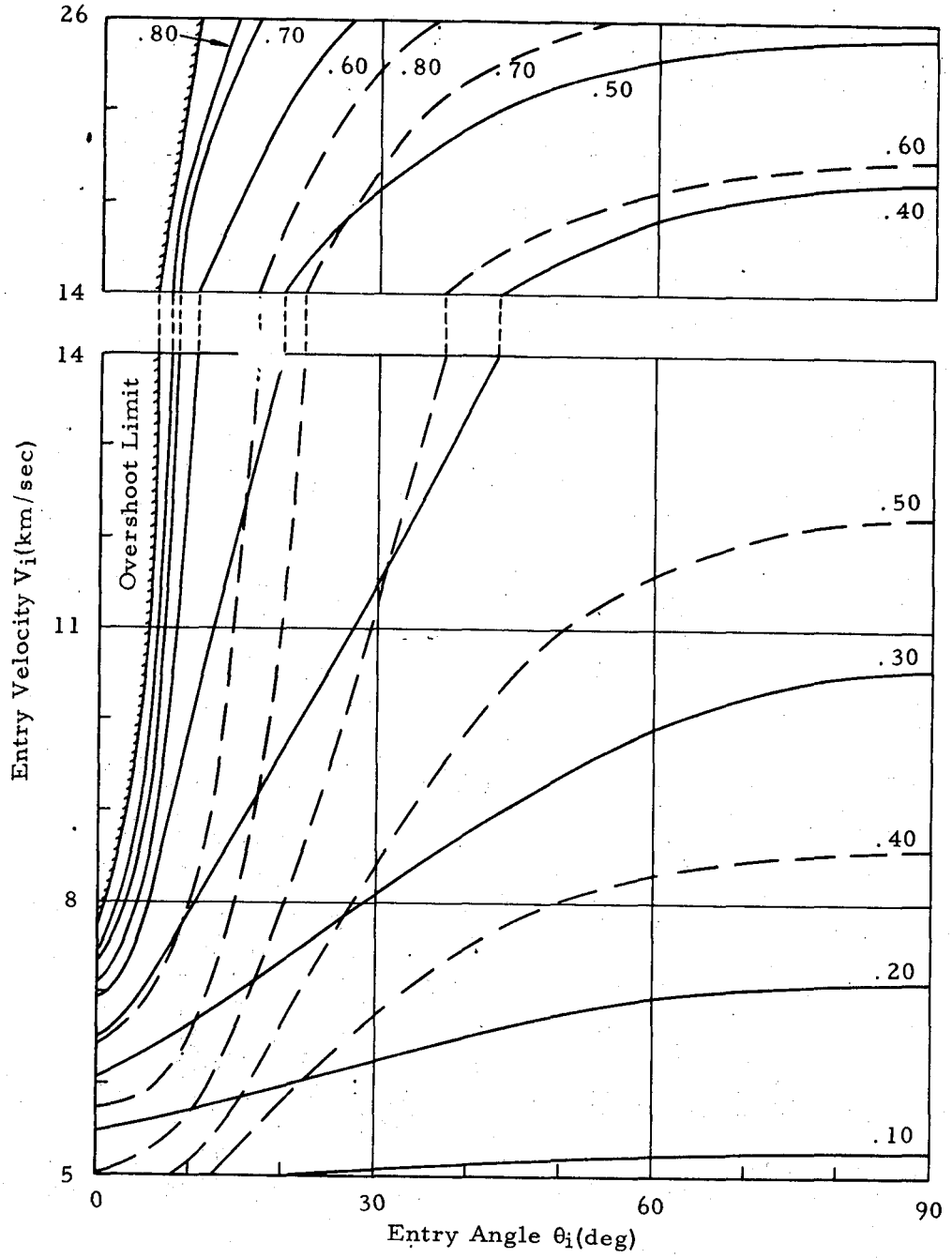

FIGURE 10: RELATIVE MASS LOSS, $1-m(t_f)/m(0)$ OF BUTTON TYPE AUSTRALITES

REFERENCES

1. Adams, Mac C. and H. A. Bethe, A Theory for the Ablation of Glassy Materials, J.Ae.Sp.Sc., Vol. 26, 1959, 321-328.

2. Adams, Ernst, Theoretical Investigation of the Ablation of a Glass Type Heat Protection Shield at the Stagnation Point of a Re-Entering Satellite, Report DA-TR-62-59, Aug. 1959.

3. Adams, Ernst, Theoretical Investigation of the Ablation of a Glass Type Heat Protection Shield at the Stagnation Point of a Re-Entering Missile, Report DA-TR-63-59, Aug. 1959.

4. Adams, Ernst, Calculation of the Transient Molten Film in the Vicinity of the Forward Stagnation Point on the Surface of a Vehicle Descending Through the Atmosphere, Report DA-TM-81-59, June 1959.

5. Adams, Ernst, Calculation Method for the Transient Melting Process of a Glassy Heat Protection Shield in the Vicinity of the Stagnation Point of a Reentry Vehicle, Report DA-TR-8-60, March 1960.

6. Adams, Ernst, A New Concept for Calculating Thermal Boundary Layers, J. Ae. Sp. Sc., vol. 27, pp. 549 - 550, 1960.

7. Adams, Ernst, The Thickness of a Melting Ablation-Type Heat Shield, J. Ae. Sp. Sc., vol. 27, pp. 620 - 621, 1960.

8. Adams, Ernst, Radiation Versus Mass-Transfer Effects for Ablating Reentry Shields of a Nonlifting Satellite, J. Ae. Sp. Sc., vol. 27, pp. 686 - 869, 1960.

9. Adams, Ernst, A Comparison of Transient and Quasi-Steady Performance of Melting-Type Reentry Shields, J. Ae. Sp. Sc., pp. 791 - 792, 1960.

10. Adams, Ernst, Theoretical Investigations of the Ablation of a Glass-Type Heat Protection Shield of Varied Material Properties at the Stagnation Point of a Reentering IRBM, NASA Tech. Note D-564, Washington, Jan. 1961.

11. Adams, Ernst, A One-Dimensional Calculation Method for the Transient Temperature, Heat Transfer, and Ablation History at the Heated Surface of a Wall, MTP-AERO-61-68, Aug. 1961.

12. Adams, Ernst, Analysis of Quartz and Teflon Shields for a Particular Reentry Mission Proceedings of the 1961 Heat Transfer and Fluid Mechanics Institute, Stanford University Press, pp. 222 - 236, 1961.

13. Adams, Ernst, Some Detrimental Aspects of the Evaporation of a Quartz Shield for a Particular Reentry Problem, J.Ae.Sp.Sc., pp. 909 - 910, vol. 28, 1961.

REFERENCES (Cont'd)

14. Adams, Ernst, Melting-Type Heat Protection of a Ballistic Satellite Reentering the Atmosphere of the Earth, Fusees et Recherche Astronautique et Spatiale, pp. 7 - 20, Paris, 1961.

15. Adams, Ernst, A Graphical Approximation for Temperatures and Sublimation Rates at Surfaces Subjected to Small Net and Large Gross Heat Transfer Rates, J.Ae.Sp.Sc., pp. 360 - 361, vol. 29, 1962.

16. Berry, Benton, A Comparison of Four Heat Protection Materials for Shielding a Capsule Entering the Atmosphere of Mars, MTP-AERO-62-70, Sept. 1962.

17. Adams, Ernst and Huffaker, Robert, Application of Ablation Analysis to Stony Meteorites and the Tektite Problem, Nature, pp. 1249 - 1251, London, 1962, vol. 193.

18. Adams, Ernst and Huffaker, Robert, Parent Body Hypothesis for Origin of Tektites, Nature, pp. 681 - 684, vol. 195, London, 1962.

19. Adams, Ernst and Huffaker, Robert, Aerodynamic Analysis of Tektites and Their Parent Bodies, NASA Tech. Rep. R-149, 1962.

20. Adams, Ernst, Heat Transfer in Laminar Flows of Incompressible Fluid with $Pr \to 0$ and $Pr \to \infty$, NASA Tech. Note D-1527, 1963.

21. Adams, Ernst and Huffaker, Robert, Aerodynamic Analysis of Tektites and Their Parent Bodies, Space Science, North Holland Publishing Co., Amsterdam, in press.

22. Adams, Ernst, Aerodynamic Analysis of Tektites and Their Hypothetical Parent Bodies, Chapter in "Tektites", edited by J. A. O'Keefe, University of Chicago Press, in press.

23. Adams, Ernst, The Low and the High Prandtl Number Approaches for Heat Transfer in Laminar Flows of Incompressible Fluids with Constant Material Properties, Proc. 4th U.S. Nat. Congr. of Appl. Mech., ASME, 1963.

24. Warmbrod, John, Calculated Results for the Transient Heating and Melting Process of Glass Shields with Various Material Properties at the Stagnation Point of a Reentering ICBM, NASA Technical Note D-1643, 1963.

25. Chapman, D. R., Larson, H. K., and Anderson, L. A., Aerodynamic Evidence Pertaining to the Entry of Tektites into the Earth's Atmosphere, NASA Tech. Rep. R-134, 1962.

26. Kivel, B., Radiation from Hot Air and Stagnation Heating, AVCO Res. Rep. 79, 1959.

27. Sutton, G. W., The Hydrodynamics and Heat Conduction of a Melting Surface, J. Ae. Sc., 25, 1958.

28. Warmbrod, John, Calculation of an Ablation Teflon Shield for a Reentry Vehicle, MTP-AERO-62-83, 1962.

APPROVAL MTP-AERO-63-47

STUDIES ON ABLATION OF OBJECTS TRAVERSING AN ATMOSPHERE

The information in this report has been reviewed for security classification. Review of any information concerning Department of Defense or Atomic Energy Commission programs has been made by the MSFC Security Classification Officer. This report, in its entirety, has been determined to be unclassified.

W. Dahm

W. K. DAHM
Chief, Aerodynamics Analysis Branch

Geissler

E. D. GEISSLER
Director, Aeroballistics Division

DISTRIBUTION MTP-AERO-63-47

M-DIR

M-DEP-DIR

M-AERO
Dr. Geissler
Mr. Dahm
Dr. Cheng
Mr. Lindsley
Mr. Wilson
Mr. Struck
Mr. Horn
Mr. Warmbrod
Dr. Adams (5)
Mr. Berry
Mr. Huffaker
Mr. Cooper
Mr. Elkins

M-P&VE
Dr. Lucas
Mr. Pool
Mr. Head
Mr. Uptagraft
Mr. Connell
Mr. Fellenz

M-MS-IP

M-MS-IPL (8)

M-PAT

M-HME-P

M-MS-H

Scientific and Technical Information Facility (2)
ATTN: NASA Representative (S-AK/RKT)
P. O. Box 5700
Bethesda, Maryland